Proc. Natl. Acad. Sci. USA
Vol. 91, pp. 9485–9489, September 1994
Cell Biology

Diffusion of inositol 1,4,5-trisphosphate but not Ca^{2+} is necessary for a class of inositol 1,4,5-trisphosphate-induced Ca^{2+} waves

M. SALEET JAFRI* AND JOEL KEIZER*†

*Institute of Theoretical Dynamics and †Section on Neurobiology, Physiology, and Behavior, University of California, Davis, CA 95616

Communicated by John Ross, June 3, 1994 (received for review January 25, 1994)

ABSTRACT **Combining a realistic model of inositol 1,4,5-trisphosphate (IP_3)-induced Ca^{2+} oscillations with the diffusion of IP_3 and buffered diffusion of Ca^{2+}, we have found that diffusion of Ca^{2+} plays only a minor role in a class of agonist-induced Ca^{2+} wave trains. These waves are primarily kinematic in nature, with variable wavelengths and speeds that depend primarily on the phase differences between oscillators at different spatial points. The period is set by the steady-state value of IP_3, while the wave speed approximately equals the wavelength/period. Ca^{2+} diffusion, which is much slower than that of IP_3 because of endogenous buffers, is shown to have only a small effect on the wave trains and not to be necessary for the apparent wave propagation. Diffusion of IP_3 sets the phase gradient responsible for these wave trains, which consist primarily of localized cycles of Ca^{2+} uptake and release. Our results imply a possible previously undisclosed role for IP_3 in cell signaling.**

Repetitive Ca^{2+} waves have been observed with fluorescent dye microscopy in a number of cell types (1, 2). In immature *Xenopus* oocytes (3), these waves are associated with the inositol 1,4,5-trisphosphate (IP_3) signal transduction pathway, and Clapham, Lechleiter and colleagues (4) have documented a rich variety of dynamical patterns and spiral waves generated by nonhydrolyzable analogues of IP_3. In hamster eggs, experiments have demonstrated that inactivating the IP_3 receptor/Ca^{2+} channel (IP_3R) with monoclonal antibodies is sufficient to eliminate fertilization-induced Ca^{2+} waves (5). These and other results imply a key role for IP_3 in Ca^{2+}-wave generation in oocytes and egg cells. Recent experiments with pituitary gonadotrophs (6) and pancreatic acinar cells (7, 8) suggest that similar mechanisms also may be functioning in these secretory cells.

Although the biological function of Ca^{2+} waves is not known, their ubiquity in certain cell types, including fertilized egg cells (5), makes understanding their mode (or modes) of propagation an important problem. Because the effective diffusion constant for Ca^{2+} is much smaller than that of IP_3 (9), it has been argued that diffusion of Ca^{2+} can explain the speed of the wave (10), and recently mathematical models have been used to explore the role of diffusion in these waves (4, 11, 12). Here we report calculations with a realistic model of IP_3-induced Ca^{2+} oscillations (13), which when combined with the diffusion of Ca^{2+} and IP_3 can generate wave trains that are primarily kinematic in nature—i.e., they do not require bulk movement of Ca^{2+} (14–16). As we describe in the following sections, the reason for this, perhaps surprising, result is the slow rate of Ca^{2+} diffusion caused by endogenous Ca^{2+} buffers.

The Model

We have based our computer simulations on a kinetic model of the biphasic Ca^{2+}-activation and -inhibition of the IP_3R (13). When combined with a sarcoplasmic or endoplasmic reticulum Ca^{2+}-ATPase (SERCA-type Ca^{2+}-ATPase) and a slow leak from the endoplasmic reticulum (ER), the model gives rises to spontaneous cytoplasmic Ca^{2+} oscillations at fixed, physiological levels of IP_3 (13). We use a simplified version of that model (17) [along with buffered diffusion of cytoplasmic Ca^{2+} (18) and the diffusion, generation, and removal of IP_3] to explore the behavior of planar Ca^{2+} waves. It is known that buffers greatly reduce the rate of diffusion of Ca^{2+} in the cytoplasm (9), and our model includes the effect of buffers in both the cytoplasm and ER (18). Fig. 1 shows a diagram of the model of Ca^{2+} handling by the ER. Ca^{2+} enters the cytosol from the ER via IP_3Rs and a leak flux, with the ER being refilled by SERCA-type Ca^{2+}-ATPases. In addition to these processes, we include Ca^{2+} diffusion in the cytosol and ER as modified by mobile and stationary Ca^{2+}-binding proteins (18). The flux into the ER is given by

$$J_{\text{pump}} = \frac{v_3[Ca^{2+}]^2}{[Ca^{2+}]^2 + k_3^2}, \qquad [1]$$

and the flux through the IP_3R and the leak from the ER are given by

$$J_{IP_3R+\text{leak}} = (v_2 + v_1 X_{110}^3)([Ca^{2+}]_{ER} - [Ca^{2+}]), \qquad [2]$$

where $[Ca^{2+}]$ is the calcium molar concentration; v_1, v_2, and v_3 are the maximum Ca^{2+} channel flux, Ca^{2+} leak flux constant, and Ca^{2+}-ATPase maximum Ca^{2+} uptake rate, respectively; k_3 is the activation constant for the Ca^{2+}-ATPase; and the term X_{110} represents the fraction of subunits of the IP_3R that are activated by IP_3 and Ca^{2+} and not inhibited by Ca^{2+} (see Fig. 1). Diffusion of Ca^{2+} is described by

$$J_{\text{dif}} = D_{Ca}\frac{\partial^2[Ca^{2+}]}{\partial x^2} + \gamma D_{CaM}\frac{\partial^2[Ca^{2+}]}{\partial x^2} - \left(\frac{2\gamma D_{CaM}}{K_m + [Ca^{2+}]}\right)\left(\frac{\partial^2[Ca^{2+}]}{\partial x^2}\right), \qquad [3]$$

where D_{Ca} and D_{CaM} are diffusion constants for free Ca^{2+} and Ca^{2+} bound to mobile endogenous buffers, respectively, and x is position in μm. The factor

$$\gamma = \frac{K_m[B_m]_T}{(K_m + [Ca^{2+}])^2} \qquad [4]$$

in the second and third terms in Eq. 3, where $[B_m]_T$ is the total concentration of mobile buffer and K_m is the dissociation constant of Ca^{2+} from the mobile buffer, accounts for the

The publication costs of this article were defrayed in part by page charge payment. This article must therefore be hereby marked "*advertisement*" in accordance with 18 U.S.C. §1734 solely to indicate this fact.

Abbreviations: IP_3, inositol 1,4,5-trisphosphate; IP_3R, IP_3 receptor/Ca^{2+} channel; ER, endoplasmic reticulum; SERCA, sarcoplasmic and endosplasmic reticulum Ca^{2+}-ATPase.

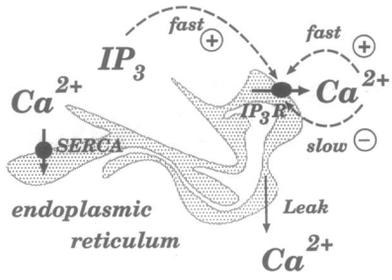

FIG. 1. Schematic diagram of the model. Ca^{2+} enters the cytosol from the ER via a passive leak and via the IP_3R, which is activated by both Ca^{2+} and IP_3 on a fast time scale and inhibited by Ca^{2+} on a slow time scale, all at the cytoplasmic face. The ER is refilled by a SERCA-type Ca^{2+}-ATPase pump. Diffusion of Ca^{2+} in both the cytosol and ER is modulated by mobile and stationary buffers (not illustrated).

transport of Ca^{2+} bound by the mobile buffers (18). Adding these terms together and multiplying by the factor

$$\beta = \left\{ 1 + \frac{K_s[B_s]_T}{(K_s + [Ca^{2+}])^2} + \frac{K_m[B_m]_T}{(K_m + [Ca^{2+}])^2} \right\}^{-1}, \quad [5]$$

where K_s and $[B_s]_T$ refer to dissociation constant of Ca^{2+} from the stationary buffer and the total concentration of the stationary buffer, to account for the remaining effects of buffering (18) yields the balance equation for $[Ca^{2+}]$:

$$\frac{\partial[Ca^{2+}]}{\partial t} = \beta(c_1 J_{IP_3R+leak} - J_{pump} + J_{dif}), \quad [6]$$

with c_1 as the fraction of cell volume that is ER and t as time of the simulation in s. Similarly the balance equation for $[Ca^{2+}]_{ER}$ is

$$\frac{\partial[Ca^{2+}]_{ER}}{\partial t} = \beta_{ER}(-J_{IP_3R+leak} + J_{pump}/c_1 + J_{dif}^{ER}), \quad [7]$$

where the superscript ER refers to comparable quantities in the ER. The concentration of IP_3, $[IP_3]$, relaxes to its steady-state value $[IP_3]^{ss}$ at the rate I_r, where $[IP_3]^{ss}$ is the IP_3 level where production balances degradation. Thus, the balance equation for IP_3 is

$$\frac{\partial[IP_3]}{\partial t} = -I_r([IP_3] - [IP_3]^{ss}) + D_{IP_3}\frac{\partial^2[IP_3]}{\partial x^2}. \quad [8]$$

To a good approximation, the time rate of change of the IP_3R subunit state, X_{110}, that determines the flux of Ca^{2+} through the IP_3R in Eq. 2 can be written (17) as follows:

$$\frac{dX_{100}}{dt} = -20.2[Ca^{2+}]X_{100} + 1.67X_{110} \quad [9]$$

$$\frac{dX_{110}}{dt} = -(0.2 + 1.67[Ca^{2+}])X_{110} + 20[Ca^{2+}]X_{100} + 0.05[IP_3]^{ss}, \quad [10]$$

where X_{100} is the fraction of subunits of the IP_3R with only IP_3 bound. In these equations, the unit of time is s, and unless otherwise noted, initial values of variables are $[Ca^{2+}] = 0.054$ μM, $[IP_3] = 0.28$ μM, $[Ca^{2+}]_{ER} = 10.95$ μM, $X_{100} = 0.33$, and $X_{110} = 0.22$.

The parameter values in these equations are given in the legend of Fig. 2 unless stated otherwise and are based on

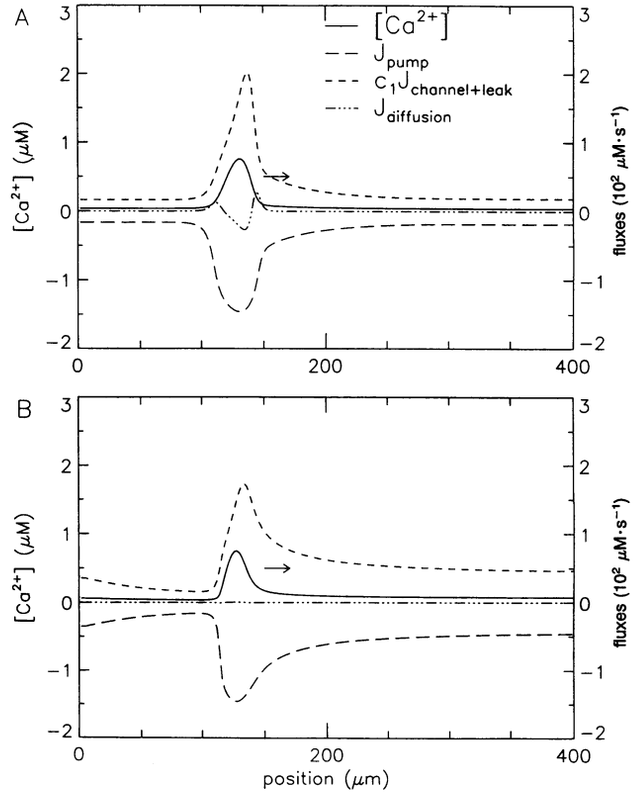

FIG. 2. Waves and fluxes generated by a 10-μM rectangular pulse of IP_3 in the left 5 μm of the domain; $[IP_3]^{ss} = 0.26$ μM. Arrows indicate the direction of propagation when shown. (*A*) Wave form and fluxes calculated with Ca^{2+} diffusion at $t = 70$ s. (*B*) Same as *A* except there is no Ca^{2+} diffusion and $t = 90$ s. Parameter values for fluxes (13): $v_1 = 300\ s^{-1}$, $v_2 = 2.0\ s^{-1}$, $v_3 = 45$ $\mu M \cdot s^{-1}$, $k_3 = 0.1$ μM, and $c_1 = 0.185$; for buffering (9, 17, 19): $K_m = 6$ μM, $[B_m]_T = 75$ μM, $K_s = 10$ μM, $[B_s]_T = 225$ μM, $K_m^{ER} = 6$ μM, $[B_m]_T^{ER} = 250$ μM, $K_s = 1$ mM, and $[B_s]_T^{ER} = 100$ mM; for diffusion (9, 18): $D_{IP_3} = 283$ $\mu m^2 \cdot s^{-1}$, $D_{Ca} = 223$ $\mu m^2 \cdot s^{-1}$, $D_{CaM} = 75$ $\mu m^2 \cdot s^{-1}$, $D_{Ca}^{ER} = 223$ $\mu m^2 \cdot s^{-1}$, and $D_{CaM}^{ER} = 75$ $\mu m^2 \cdot s^{-1}$; and for IP_3 (13): $[IP_3]^{ss} = 0.26$ μM, $I_r = 0.05\ s^{-1}$. Calculations in the absence of Ca^{2+} diffusion were carried out with all diffusion constants set equal to zero.

previous work. Parameters for Ca^{2+} buffering are in the range suggested by experiments with cytoplasmic extracts from *Xenopus laevis* oocytes (9) and give an effective diffusion constant for Ca^{2+} (17) of about 31 $\mu m^2 \cdot s^{-1}$ in the cytoplasm and 6 $\mu m^2 \cdot s^{-1}$ in the ER. The smaller value in the ER results from the higher concentration of buffers there, in agreement with experimental estimates (19). Parameters for the kinetics of Ca^{2+} uptake and release via the SERCA pump and the IP_3R are based on a variety of kinetic experiments as described (13).

Effect of Diffusion on Ca^{2+} Waves

Our calculations started with spatially uniform initial conditions on a domain consisting of a straight line 500 μm long. [Numerical integration of the model was performed by using an implicit finite difference method ($dx = 0.1$, $dt = 0.01$) on a SGI Indigo work station. The time step was changed to $dt = 0.02$ to calculate the fluxes in Fig. 4. Graphics were generated by using PV-WAVE by Precision Visuals.] The steady-state concentration of IP_3, $[IP_3]^{ss}$, was set so that in the absence of diffusion the entire domain would oscillate synchronously. A 10 μM rectangular pulse of IP_3 was then applied in the 5-μm region at the left boundary. This initiates the passage of the first wave of Ca^{2+} that crosses somewhat more than half of the domain and then terminates in a bulk

oscillation on the right-hand side. As time progresses, this transient behavior dies out, and each succeeding wave propagates across the entire domain, forming one peak in a steady wave train. A typical peak of the wave train is shown at t = 70 s in Fig. 2*A*, along with the various contributions in Eq. 6 to the time derivatives ("fluxes") of the Ca^{2+} concentration. Note that the diffusive flux, J_{dif}, is small compared with the other fluxes and changes sign twice, where the second derivative of the Ca^{2+} concentration vanishes. The small size of J_{dif} led us to repeat these calculations with Ca^{2+} diffusion eliminated by setting the diffusion constants for Ca^{2+} and Ca^{2+} bound to mobile buffer equal to zero. This produced a very similar train of Ca^{2+} waves (Fig. 2*B*) in spite of the fact that J_{dif} is identically zero. These results are typical of many calculations with differing pulse shapes and oscillatory conditions. Thus, diffusion of Ca^{2+} in the cytosol and in the ER appears to be unnecessary for generation and propagation of these wave trains.

If diffusion of Ca^{2+} is not necessary for these waves, why do they occur? The key is the rapidity of diffusion of IP_3 compared with that of Ca^{2+} (9). Indeed, when the diffusion of IP_3 is eliminated from the same calculations, then neither the Ca^{2+}-diffusion-assisted nor Ca^{2+}-diffusion-independent wave trains in Fig. 2 are generated by pulses of IP_3. To understand the effect of IP_3 diffusion, we have calculated the time course of Ca^{2+} and IP_3 following a pulse of IP_3 at a fixed position in space (Fig. 3 *A* and *B*). Within 50 s the $[IP_3]$ returns to its steady-state value because of losses by diffusion and removal (Fig. 3*C*) (N. L. Allbritton, personal communication). During this period diffusion carries IP_3 across the spatial domain, systematically perturbing the oscillations at each point. The perturbation is largest near the left boundary where the pulse was administered. After approximately 50 s, the amplitude and frequency of the oscillations return to their initial values. In the process, however, differences in the relative positions of oscillators in their cycles (their "phases") occur, with points on the left being "ahead" of neighboring points on the right. This "phase gradient" leads to an apparent wave train traveling to the right, even in the absence of Ca^{2+} diffusion. Recent experiments (N. L. Allbritton, personal communication) suggest that the rate of removal of IP_3 is slow enough for IP_3 to diffuse across the length of a cell. This allows the phase gradient described above to cover the entire domain.

A schematic diagram of this type of wave (a "phase" or "kinematic" wave) is drawn in Fig. 4, where the oscillation at each point in space is represented by a clock. The period, τ, of the oscillation is the time required for the hand to make

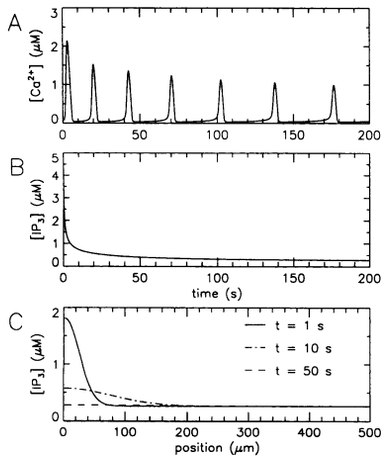

FIG. 3. The time course of $[Ca^{2+}]$ (*A*) and $[IP_3]$ (*B*) flux for a point 5 μm from the left boundary. Same conditions as Fig. 2*A* except that I_r = 0.01 s^{-1}. (*C*) Spatial profile of $[IP_3]$ at t = 1, 10, and 50 s (I_r = 0.05 s^{-1}).

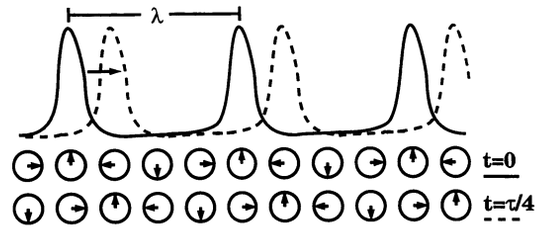

FIG. 4. Illustrating a kinematic wave with "clocks"; the peak of the wave is drawn to coincide with the hand of the "clock" pointing at 12:00. The period (τ) is the time it takes for the hand at a given location to make one complete clockwise revolution, with adjacent clocks out of phase one-quarter period. The minimum distance between two different clocks with the same phase is the wavelength (λ). A wave takes τ seconds to travel one wavelength, so that wave speed $c = \lambda/\tau$. The wave at t = 0 (solid curve) progresses one-quarter of a wavelength at $t = \tau/4$ (dashed line).

one revolution, and the wavelength, λ, is the distance between clocks with hands pointing in the same direction. A brief study of the figure shows that the time it takes a phase wave to travel one wavelength is one period and that the wave speed, c, is given by $c = \lambda/\tau$. Because the wavelength of a phase wave is determined by the local phase gradient, both λ and the c can vary from one region to another. In Fig. 4, the phase gradient results in a wave train moving to the right.

Testing the Importance of Ca^{2+} Diffusion

To test quantitatively the notion that these wave trains are predominantly phase waves, we measured λ and c for waves produced by an initial linear ramp of IP_3. In contrast to diffusion-dependent waves (14), these quantities can be changed arbitrarily for phase waves by altering the phase gradient. Fig. 5 shows that with other properties held fixed, both the wave speed and the wavelength are determined by the size of the ramp used to initiate them. The triangles and circles give the value of the wave speed and wavelength measured near the center of the domain. The value of $[IP_3]$ at the left boundary was above that at the right boundary, which was set at 0.25 μm for the steady-state level of both 0.26 μM (triangles) or 0.52 μM (circles). In both cases the higher the initial value at the left boundary, the lower was the wave speed and the shorter the wavelength. The correlation is linear and agrees well with the relationship $c = \lambda/\tau$, which is expected for phase waves (see Fig. 4), where τ = 43.7 s at $[IP_3]^{ss}$ = 0.26 μM and 20.6 s at $[IP_3]^{ss}$ = 0.52 μM. The range of wavelengths and speeds in Fig. 5 is in agreement with that reported in a variety of cells (1). Elimination of Ca^{2+} diffusion from the calculations (open symbols) had very little effect on the wavelengths and increased the wave speed by <1 $\mu m \cdot s^{-1}$.

We have also generated kinematic wave trains of Ca^{2+} using pulses of Ca^{2+} (30 μm wide, 0.4 μM). The initial pulse of Ca^{2+} starts a propagating wave train when $[IP_3]^{ss}$ has a value in the oscillatory range. While the first wave in the train requires Ca^{2+} diffusion for its propagation, subsequent waves continue to propagate in the absence of Ca^{2+} diffusion (not shown). For these waves it is the initial diffusion of Ca^{2+} that resets the phases of the oscillators, setting up conditions for the kinematic wave train.

In experiments with *Xenopus* oocytes, a collision between two Ca^{2+} waves results in their annihilation. This behavior is reproduced by our calculations in Fig. 6, which shows the progress of waves resulting from a V-shaped ramp of IP_3 (5.25 μM at the edges and 0.25 μM at the middle). The ramp initiates wave trains emanating from the boundaries and traveling towards the center where they collide. The nature of the collision provides another measure of the minor role that Ca^{2+} diffusion plays in the waves. Indeed, in pure phase

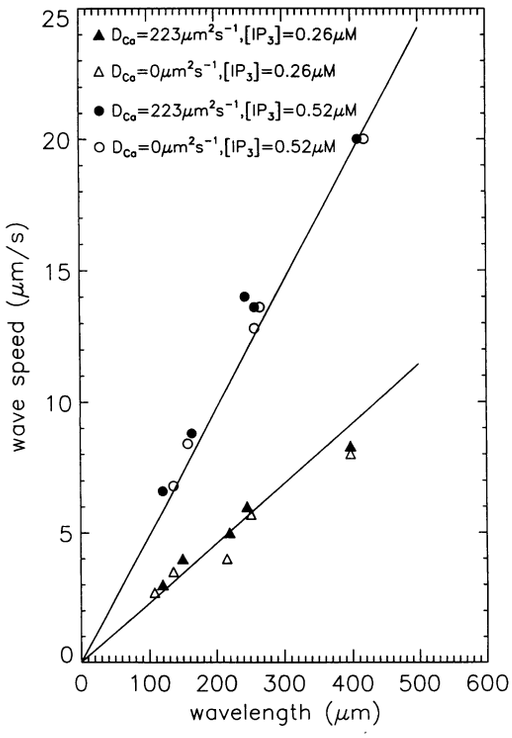

FIG. 5. Wave speed is related to wavelength by $c = \lambda/\tau$. Waves are generated by a linear ramp of initial $[IP_3]$ (high at left boundary, steady state at right boundary). Triangles and circles represent $[IP_3]^{ss}$ = 0.26 and 0.52 μM, respectively, with filled symbols in the presence and open symbols in the absence of Ca^{2+} diffusion. Different wavelengths were obtained by varying $[IP_3]$ at the left boundary. Straight lines were drawn by using $c = \lambda/\tau$ with τ = 20.6 s for $[IP_3]^{ss}$ = 0.52 μM and τ = 43.7 s for $[IP_3]^{ss}$ = 0.26 μM.

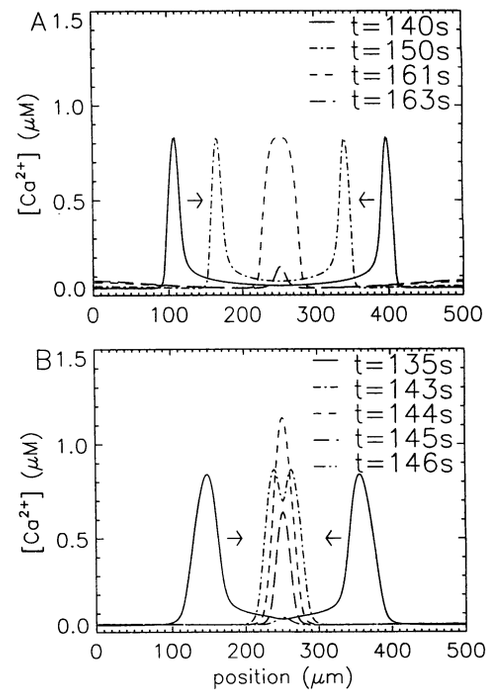

FIG. 6. Collision of waves initiated from a V-shaped ramp of initial $[IP_3]$ of 1.5 μM at x = 0 μm and x = 500 μm that descend linearly to 0.25 μM at x = 250 μm and x = 250.1 μm. The two waves start at the edges, collide in the middle, and annihilate. (*A*) With no diffusion of Ca^{2+}, there is no reinforcement upon collision at t = 161 s. (*B*) With Ca^{2+} diffusion, there is a small increase in $[Ca^{2+}]$ when waves collide at t = 144 s.

waves, a "collision" involves no mass transport and, therefore, no change of amplitude at the moment of collision (Fig. 6*A*) prior to annihilating each other. When the same calculation is repeated in the presence of Ca^{2+} diffusion (Fig. 6*B*), the collision is accompanied by only a slight increase in amplitude that results from the additive contributions of J_{dif} in the wave fronts (see Fig. 2). We conclude that the existence of the waves and their qualitative behavior do not depend critically on the diffusion of Ca^{2+}.

The occurrence of waves in which Ca^{2+} diffusion plays a minor role is not due to some peculiarity of our choice of model. We have repeated these calculations using two other models of IP_3R-based Ca^{2+} oscillations (6, 10), both of which produce phase waves similar to those seen in Fig. 2. Those calculations also included the disparity between the diffusion coefficients of Ca^{2+} and IP_3, reinforcing our conclusion that it is this difference that helps to create these waves. Nor are these waves due to a specific choice of initial conditions. When the initial conditions are varied to give spatial heterogeneity of the initial states, waves can be produced by the same protocols as before. Kinematic waves of a related sort are well-known in other systems, including the Belousov–Zhabotinskii reaction (15), where they are a consequence of slow diffusion of one or more substances.‡ Based on these results, we conclude that phase gradients, rather than Ca^{2+} diffusion, may play a significant role in the propagation of certain wave trains of cellular Ca^{2+}, with diffusion of IP_3 responsible for setting the gradient.

Other types of Ca^{2+} waves also exist in excitable and oscillatory models of Ca^{2+} handling, including diffusion-based solitary (or trigger) waves and wave trains (4, 10, 11). These types of waves require diffusion of Ca^{2+}, can be initiated by Ca^{2+} pulses, and have wave speeds that are generally proportional to the square root of the Ca^{2+} diffusion constant (14). We have verified that both types of these diffusion-based waves can be generated by our model (not shown). However, diffusion-dependent trigger waves can be generated only at concentrations of IP_3 close to the threshold for oscillations. Having explored a range of parameters in our model, our experience is that repetitive waves, like those seen in Figs. 2*A* and 6*B* for which Ca^{2+} diffusion is not necessary for propagation, are easily generated as long as the medium is oscillatory.

Relation to Experiment

There are important differences between waves that are dependent on Ca^{2+} diffusion and waves that are primarily independent of Ca^{2+} diffusion. For the latter class of waves, we have shown that the wave speed can be varied by varying the conditions that generate the waves. We have also shown that the relationship $c = \lambda/\tau$ holds for this type of wave. Since this simple dispersion relation is not valid for diffusion-dependent waves, it should be possible to distinguish the two types of waves by modifying systematically the period of the oscillations and measuring the wavelength and wave speed. Although detailed experiments of this sort have not been reported, Camacho and Lechleiter (20) have published data on the effect of the expression of the SERCA-1 pump on Ca^{2+} waves in *Xenopus* oocytes. Given that this change decreased

‡The underlying theory of these waves can be couched in terms of the two-timing analysis of Murray (14), which suggests that slow diffusion perturbs the amplitude of the oscillators only slightly. Furthermore, at short times the distribution of phase is determined by initial gradients, while at longer times the phase evolves according to Burgers' equation. In the present context, the rapid diffusion of IP_3 can be thought of as setting the distribution of phases on the short time scale.

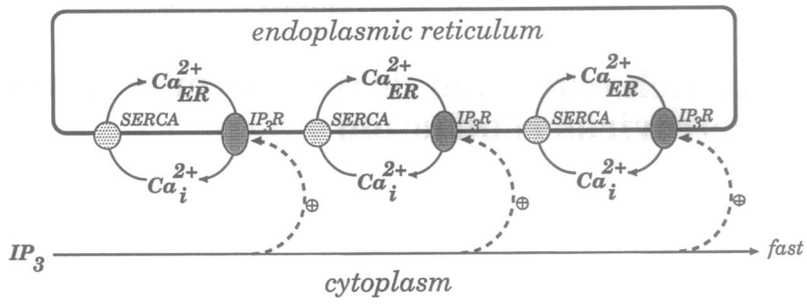

FIG. 7. Schematic representation showing how the phase of localized oscillations in Ca^{2+} uptake and release from the ER can be set by the rapid diffusion of IP_3. Diffusion of Ca^{2+}, which is of minor importance in the propagation of the wave, is not shown.

the period of the oscillations and had no effect on the wave speed, $c = \lambda/\tau$ correctly predicts the observed decrease in wavelength. A more systematic way to test this relationship might be to add a mixture of exogenous stationary and mobile buffers to the cell. By choosing the correct combination, it should be possible to decrease the buffering factor β in Eq. 6 without appreciably altering the diffusion term in Eq. 3. Our calculations have shown that decreasing β in this fashion will lengthen the period of the oscillations.

Recent experiments in pancreatic acinar cells have provided evidence that IP_3-generated Ca^{2+} waves (stimulated by agonist applied to the apical pole) initiate at the basolateral membrane (8). In these cells there is convincing evidence that the concentration of IP_3 rises before that of Ca^{2+} and that rapid diffusion of IP_3 from the apical pole initiates these waves. In the model of Ca^{2+} handling by the ER used here, it is known (13) that increasing the IP_3 concentration decreases the period of Ca^{2+} oscillations, in general agreement with previous observations (2). Using graded doses of agonist and measuring the period, wavelength, and wave speed would provide another way of testing $c = \lambda/\tau$. Finally, if a Ca^{2+} wave were predominately kinematic, then we predict that differing initiating pulses or ramps of IP_3 should lead to different wave speeds. It should be possible to test this prediction by using photoreleased (caged) IP_3 in the presence of oscillatory amounts of agonist. In that case, longer photorelease pulses should lead to slower wave speeds if the diffusion of Ca^{2+} were of minor importance.

Conclusions

Our calculations, using a realistic model of Ca^{2+} handling by the ER and a description of Ca^{2+} diffusion that is appropriate to the highly buffered cytosolic and ER compartments, suggest that Ca^{2+} waves that occur under oscillatory conditions are predominately kinematic. This implies that the diffusion of Ca^{2+} is not necessary for propagation of the wave. Because the diffusion constant of Ca^{2+} in the cytosol is now known to be smaller than that of IP_3 by about 1 order of magnitude (8, 9), we propose that propagation of Ca^{2+} waves can occur even if there is only localized oscillatory release and reuptake of Ca^{2+} from the ER. In this scenario, adjacent spatial regions oscillate with slightly different phases set by IP_3 as it diffuses from a localized pulse. An illustration of this mechanism of propagation is given in Fig. 7.

We have used our calculations to test whether or not initial spatial inhomogeneities in phase of these oscillations can be reset by a pulse of IP_3 and find that after a short transient period, the pulse of IP_3 succeeds in producing a coordinated wave train. This would not be true, of course, if there were significant inhomogeneities in the spatial distribution of the Ca^{2+} uptake and release channels in the ER. However, such inhomogeneities, which appear to exist in acinar cell (7, 8), might serve a similar function to IP_3 diffusion in coordinating the phase of local oscillations. Indeed, if the density of uptake and release channels varies throughout a cell, the period of the local oscillators would differ from place to place. Similarly a spatial gradient of IP_3, caused by localized production of IP_3 at restricted portions of the plasma membrane, could conspire with diffusion and breakdown of IP_3 to produce a spatial distribution of oscillator periods. Either of these possibilities could, in principle, create a related type of kinematic Ca^{2+} wave of the sort described in the Belousov–Zhabotinskii reaction by Kopell and Howard (15).

What implications do predominately kinematic waves have for cell signaling? First, even when mass transport of Ca^{2+} is slow, they permit IP_3 to create a signal with all of the potentially useful properties of a wave—i.e., a wave speed, wavelength, and direction of propagation. Second, persistence of the phase gradient might provide a short-term global memory of the point of origin of the initiating IP_3 signal and a simple way to erase the memory by initiation of a signal from a separate location. Finally, because the wavelength and speed of the wave train depend on the amplitude of the initiating signal, this type of wave can encode amplitude information about the initial stimulus, something that does not occur with diffusion-dependent waves.

We thank John Wagner, Greg Smith, and Nancy Koppell for helpful conversations and John Rinzel and Richard Nuccitelli for critiquing the manuscript. This work was supported by National Science Foundation Grants BIR 9300799 and BIR 9214381 and the University of California Agricultural Experiment Station.

1. Jaffe, L. (1991) *Proc. Natl. Acad. Sci. USA* **88**, 9883–9888.
2. Berridge, M. J. (1993) *Nature (London)* **361**, 315–325.
3. Lechleiter, J. D. & Clapham, D. E. (1992) *Cell* **69**, 283–291.
4. Girard, S., Lückhoff, A., Lechleiter, J., Sneyd, J. & Clapham, D. H. (1992) *Biophys. J.* **61**, 509–517.
5. Miyazaki, S., Shirakawa, H., Nakada, K. & Honda, Y. (1993) *Dev. Biol.* **158**, 62–78.
6. Li, Y.-X., Rinzel, J., Keizer, J. & Stojilković, S. (1994) *Proc. Natl. Acad. Sci. USA* **91**, 58–62.
7. Thorn, T., Lawrie, A., Smith, P., Gallacher, D. & Petersen, O. (1993) *Cell Calcium* **14**, 746–757.
8. Gromada, J., Jørgensen, T., Tritsaris, K., Nauntofte, B. & Dissing, S. (1993) *Cell Calcium* **14**, 711–723.
9. Allbritton, N. L., Meyer, T. & Stryer, L. (1992) *Science* **258**, 1812–1815.
10. Atri, A., Amundson, J., Clapham, D. & Sneyd, J. (1993) *Biophys. J.* **65**, 1727–1739.
11. Dupont, G. & Goldbeter, A. (1992) *BioEssays* **14**, 485–493.
12. Othmer, H. G. & Tang, Y. (1993) in *Experimental and Theoretical Advances in Biological Pattern Formation*, eds. Othmer, H. G., Maini, P. K. & Murray, J. D. (Plenum, New York).
13. De Young, G. & Keizer, J. (1992) *Proc. Natl. Acad. Sci. USA* **89**, 9895–9899.
14. Murray, J. (1989) *Mathematical Biology* (Springer, New York).
15. Kopell, N. & Howard, N. (1973) *Science* **180**, 1171–1174.
16. Ross, J., Müller, S. & Vidal, C. (1988) *Science* **240**, 260–265.
17. Keizer, J. & De Young, G. (1994) *J. Theor. Biol.* **166**, 431–442.
18. Wagner, J. & Keizer, J. (1994) *Biophys. J.* **67**, 447–456.
19. Somlyo, A., Bond, M. & Somlyo, A. (1985) *Nature (London)* **314**, 622–625.
20. Camacho, P. & Lechleiter, J. D. (1993) *Science* **260**, 226–229.